A theoretical study of solid hydrogens doped with atomic oxygen

Zhiming Li and V. A. Apkarian
Department of Chemistry, University of California, Irvine, California 92697-2025

Lawrence B. Harding
Theoretical Chemistry Group, Argonne National Laboratory, Argonne, Illinois 60439

(Received 18 July 1996; accepted 8 October 1996)

Structure and reaction dynamics in solid H_2/D_2 doped with $O(^3P, ^1D, ^1S)$ is investigated through simulations based on accurate *ab initio* potential energy surfaces. The *ab initio* calculations are performed at MCSCF level, with neglect of spin–orbit interactions. The dynamical simulations rely on nonadditive effective potentials, taking into account the anisotropy of the open shell atom by using diabatic representations for the globally fitted potential energy surfaces of $O-H_2$. The ground state of the doped solid is well described as $O(^3P)$ isolated in para-$H_2(J=0)$ since the atom–molecule interaction anisotropy is not sufficient to orient H_2. $O(^3P)$ atoms radially localize the nearest-neighbor shell, and lead to a linear increase in the density of the solid as a function of impurity concentration. The doped solid is stable at cryogenic temperatures, with a free energy barrier for recombination of next nearest-neighbor $O(^3P)$ atoms of 120 K. The solid state $O(^1D)+H_2$ reaction is considered in some depth. While in high symmetry sites the reaction is forbidden, even at 4 K, thermal fluctuations are sufficient to promote the insertion reaction. © *1997 American Institute of Physics.* [S0021-9606(97)00103-7]

I. INTRODUCTION

Solid hydrogens doped with atomic oxygen have long been identified as potential cryogenic propellants with enhanced specific impulse.[1–4] Yet, little is known about the cryo-chemistry or the physical properties of such doped solids. The relevant chemistry in this case is the reactivity of the guest with the host, $O+H_2$, and the recombination of guest atoms, O+O, after detrapping. As one of the more fundamental prototypes in chemistry, the $O+H_2$ reaction has been extensively studied in the gas phase.[5,6] However, transferring of knowledge from these high temperature studies to cryogenic conditions is not straightforward. The requirements for characterization of chemistry at the cryogenic temperatures relevant to solid hydrogens, $T<10$ K, are severe with respect to the demand on accuracy of potential surfaces. As an example, it is well established that the reaction of $O(^1D)$ with H_2 has a gas kinetic cross section,[7] and most calculations agree that if a barrier exists on this surface it is of the order of kT or less.[8] Yet, evidence has been given that $O(^1D)$ atoms vertically prepared by the radiative $O(^1S)\rightarrow O(^1D)$ transition in solid hydrogen at 4 K, do not react with the host.[9] The evidence for this conclusion is based on the observation that the atomic fluorescence does not bleach. Indeed if the barrier to this reaction were of the order of 100 K, it would be perfectly ignorable in high temperature studies, and would be outside the reliability of most potential energy surface calculations. Yet, at the temperatures of relevance to solid H_2, a 100 K barrier would be insurmountable. A careful exploration on state-of-the-art potential energy surfaces was therefore deemed necessary for making reliable predictions with respect to chemistry, and to rationalize the recent experimental studies. The second reaction of concern, the O+O recombination, would be expected to be controlled by the mobility of the guests in the solid. The mobility of a classical impurity in a quantum host,[10] of which solid hydrogen is a good example; or for that matter, any molecular level description of dynamics in quantum many-body systems, presents serious conceptual challenges for which there are few tried theoretical tools. This consideration is another prime motivation for our studies.

In recent years, there has been considerable experimental and theoretical progress in studies of chromophores isolated in quantum hosts, in solid H_2,[11] in solid and superfluid He,[12] and in large clusters of He.[13] A major aim of these studies is the elucidation of structural and dynamical peculiarities of such media. As far as solid hydrogens are concerned, one of the better investigated systems has become the electronic spectroscopy of Li atom doped solid hydrogens, which was studied experimentally by Fajardo *et al.*[14] and subsequently scrutinized theoretically by several groups.[15,16] Whaley *et al.* studied the ground states of several large doped quantum clusters by quantum Monte Carlo methods.[17] Diffusion Monte Carlo methods pioneered by Anderson,[18] have been used to calculate the ground state of doped clusters, and by taking advantage of the symmetry of the node in the first excited state, the wave function for the vibrationally excited state and therefore infrared spectra of impurities isolated in clusters has been obtained.[19] The same methodology had earlier been used by Buch in calculations of mixed ortho and paraclusters of hydrogen.[20] Such simulations can be used to determine approximate line shapes for electronic excitation, and the calculations of this property were pursued for Li impurities in para-H_2 clusters,[15] and in solid hydrogen.[16] The Monte Carlo methods, in effect, are equilibrium calculations of stationary states, usually limited to the ground state.[21] A rather simple method for dynamical simulations in solid hydrogen, which incorporated the effect of zero-point energies through Gaussian convolution of pair potentials was imple-

 0021-9606/97/106(3)/942/12/$10.00

mented earlier by us, and was applied for obtaining structural and dynamical information on O_2 doped solid hydrogens.[22] Although we introduced our method in an *ad hoc* fashion, it finds justification in the centroid dynamics rigorously developed by Cao and Voth,[23] who have given an alternate method for constructing pseudo potentials,[24] and used them in simulations of liquid para-hydrogen.[25] Despite the approximate nature of our treatment, good agreement was found with the structural determinations of pure and doped hydrogens obtained by the more accurate path integral methods,[15,16] and correct predictions were made for the fluorescence polarization of O_2 isolated in solid hydrogens.[26] A further refinement of the method, based on the construction of effective potentials that reproduce not only structure but also the correct phonon spectrum, was more recently advanced in the treatment of impurity rotations in quantum solids.[22(b)] Here, we combine the method of effective potentials with a treatment of the many-body interactions of the open shell O atom, which was previously implemented in the study of oxygen atom mobilities in rare gas solids.[27] The latter treatment is based on the construction of adiabatic potential energy surfaces from experimentally determined anisotropic pair potentials.[28] The present treatment is similar in spirit, the major difference being that in the case of $O–H_2$ interactions, in addition to the angular anisotropy of the electronic distribution on the O atom, the orientational anisotropy of H_2 molecules needs to be explicitly considered. As we will argue, based on analysis of the $O–H_2$ pair, angularly averaged pair potentials are justifiable in this application. Limitation of the treatment to the $J=0$ free rotor states of H_2, renders the description of the many-body $O–H_2$ interactions to be identical in form to that of O–rare gas interactions. With the method justified, we proceed to examine the effects of the O impurity on the structure of solid H_2, mobility of $O(^3P)$ in the lattice, and reactivity of the excited $O(^1D)$ atom with the host.

The rest of the paper is organized as follows. Section II describes the *ab initio* potential surfaces, and details of the fitting procedure in a diabatic representation. Based on these surfaces, in Sec. III, we present a simple particle-in-a-ring model to establish the validity of a free rotor description of the host molecules in the presence of $O(^3P)$. With that justification, and noting that in the presence of the paramagnetic impurity the host will convert to its ground state, in the rest of the paper we treat H_2 as spherical particles. The method employed for the simulations in this limit is outlined in Sec. IV. The structural properties of $O(^3P)$ in solid D_2 and the reactivity of $O(^1D)$ in the same host are discussed in Sec. V. Conclusions are given in Sec. VI.

II. POTENTIAL ENERGY FUNCTIONS

A. *Ab initio* calculations

The calculations reported here are of the multireference, configuration interaction (MR–CI) variety, in which orbitals are first optimized using a state-averaged, multiconfiguration, self-consistent field (MCSCF) calculation and then these orbitals are used in a subsequent MR–CI calculation. To optimize the orbitals, separate, singlet and triplet, state averaged, 10 orbital, 8 electron, complete active space self-consistent field (CASSCF) calculations were carried out using the MOLPRO[29,30] program package. For the singlet surfaces, the state averaging was done over the five lowest states [corresponding to the five components of the $O(^1D)+H_2$ asymptote]. For the triplet states the state averaging was done over the three lowest states [corresponding to the three components of the $O(^3P)+H_2$ asymptote]. In all cases, all states were weighted equally in the averaging. In these calculations the 10 active orbitals consist of the oxygen $2s$, $2p_x$, $2p_y$, $2p_z$, $3s$, $3p_x$, $3p_y$, and $3p_z$ orbitals and the HH, s, and s^* orbitals. Tests using smaller active spaces were found to be unsatisfactory due to problems resolving the $1s$, $2s$, and $2p$ orbitals and/or to inequivalent p orbitals at large $R_{O–HH}$ separations. For the singlet surfaces the above CASSCF wave function includes 13 860 configurations. This is far too many configurations to use as a reference space for the CI calculations. In order to make the CI calculations feasible a smaller reference space was used consisting of a 6 orbital, 8 electron CAS in which the four lowest occupation natural orbitals from the 10 orbital CAS (corresponding to the oxygen $n=3$ orbitals) are removed from the active space. Thus the active space for the CI calculations consists of the following orbitals: oxygen, $2s$, $2p_x$, $2p_y$, and $2p_z$ and HH, s, and s^*. Tests using the MOLPRO[29,31] internally contracted CI method to do the CI calculations proved to be unsatisfactory because at large $R_{O–HH}$ separations the five components of the $O(^1D)+H_2$ asymptote were predicted to be significantly nondegenerate (apparently an artifact of the contraction scheme). Consequently it was deemed necessary to do uncontracted CI calculations using the COLUMBUS[32] program package. The effects of higher order excitations (beyond singles and doubles) were estimated using the normalized, multireference Davidson[33] correction. The calculations were carried out on a 10 processor, IBM-SP computer.

Calculations were done using three different basis sets to test the sensitivity of the results to the size of the basis set. The basis sets used are the Dunning,[34] correlation consistent, augmented, polarized double zeta, triple zeta, and quadruple zeta (aug-pvdz, aug-pvtz, and aug-pvqz) basis sets. These basis sets all include diffuse functions to improve the accuracy at large distances. All of the dynamical results reported here employ fits to results obtained with the aug-pvtz basis set. Calculations with the aug-pvdz and aug-pvqz basis sets were used only to check the convergence of the calculated relative energies with respect to changes in the basis set size. In the long-range regions of interest here only small differences were found between the aug-pvdz and aug-pvtz results. Calculations with the aug-pvqz basis set were only be done in regions of high symmetry. For the C_{2v} approach the aug-pvqz calculations were found to yield interaction energies ~ 2 cm^{-1} less attractive than the aug-pvtz calculations for $O–H_2$ distances between 5 and 8 au. For shorter distances, the aug-pvqz results become substantially more attractive than the aug-pvtz results. However, these regions are not relevant to the dynamics studied here.

Contour plots of the six singlet potential surfaces are

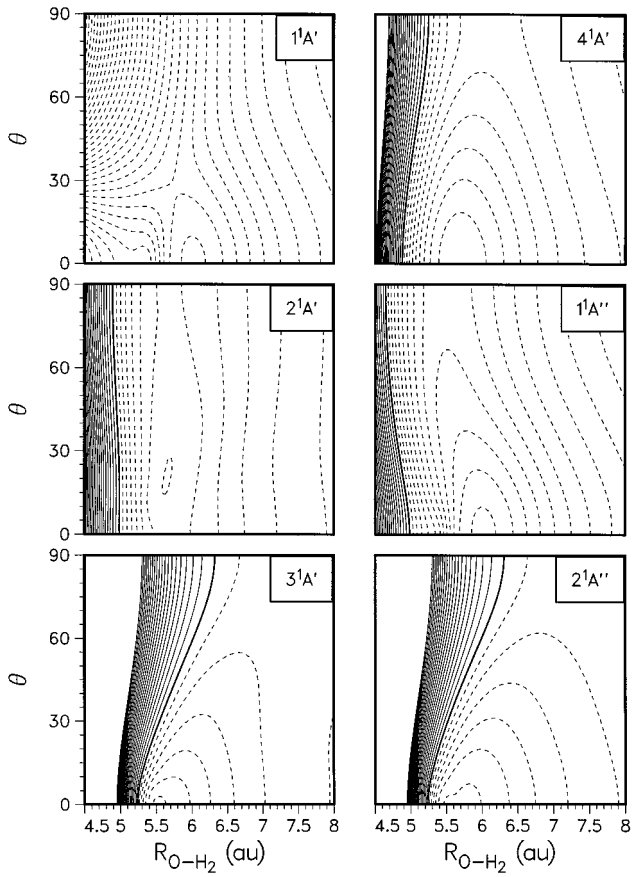

FIG. 1. Two-dimensional contour plots of the six singlet potential surfaces. The R_{HH} distance is kept fixed at its equilibrium value. The contour increment is 10 cm^{-1}. Dashed contours denote energies less than that of the $O+H_2$ asymptote (attractive). Solid contours denote energies greater than that of the asymptote.

shown in Fig. 1. In this figure the surfaces labeled, $1\,^1A'$, $2\,^1A'$, $3\,^1A'$, $1\,^1A''$, and $2\,^1A''$ correlate with $O(^1D)+H_2$, while the surface labeled $4^1A'$ correlates with $O(^1S)+H_2$. From these plots it can be seen that the lowest of these surfaces, the $1\,^1A'$ surface, is attractive in all orientations, having a shallow local minimum for linear geometries at an $O–H_2$ distance of ~6.2 a.u. The other surfaces are all attractive for all orientations at long range and repulsive for all orientations at short range. All but the $2\,^1A'$ surface are predicted to have linear minima.

B. Global fit of potential surfaces

In the absence of the spin–orbit Hamiltonian, the three distinct manifolds that arise from ^3P, ^1D, and ^1S, are separable, and will be fitted as such. To generate a global fit to these surfaces in terms of R and θ, the system is considered in C_s symmetry. The only symmetry factorization that is possible then is according to the irreducible representations A' and A'', corresponding, respectively, to the symmetric and antisymmetric representations with respect to reflection in the plane formed by the three atoms. In fitting the data to analytical functions, the oxygen atom charge distribution is represented in the limited diabatic basis sets of p_x, p_y, and p_z for the ^3P state, and $d_{z^2}, d_{xy}, d_{xz}, d_{yz}, d_{x^2-y^2}$ for the ^1D state. Detailed discussion and justification of such limited basis expansions for many-body treatments has already been given for open shell–closed shell interactions of halogen–rare gas,[35] and oxygen–rare gas,[27] interactions previously. The same would obviously suffice for treating interactions between oxygen and para-H_2(ortho-D_2). However, in fitting the *ab initio* data, it is necessary to consider the nonrotating H_2 molecule, or ortho-H_2, and therefore, a two-center electrostatic expansion serves as the proper basis set for the global fits. A good discussion of such an analysis has recently been given by Alexander *et al.* in their treatment of $B–H_2$ potentials.[36,37]

1. ^1S state

For the $O(^1S)$ state, the electron distribution on the O atom is spherically symmetric. Denoting R as the distance between the O atom and the center of mass of H_2, and θ as the angle between R and the H_2 bond, the potential energy function of the interaction between an $O(^1S)$ and H_2 molecule can be written as

$$V(R,\theta)=\sum_{L=0,2} V_L(R) D^L_{00}(0,\theta,0), \tag{1}$$

where the radial functions are assumed to be

$$V_L(R)=\frac{C_{12}}{R^{12}}+\frac{C_{10}}{R^{10}}+\frac{C_8}{R^8}+\frac{C_6}{R^6}, \tag{2}$$

and the rotation matrix is defined as[38]

$$D^L_{m0}(\alpha,\beta,0)=\sqrt{\frac{4\pi}{2l+1}}\, Y^*_{lm}(\beta,\alpha). \tag{3}$$

The numerical values of fitting parameters are available upon request[39] and the potential energy contour is same as $4\,^1A'$ in Fig. 1. The minimum energy geometry is collinear, i.e., $\theta=0$.

2. ^3P state

There are three sublevels in the ground state, $O(^3P)–H_2$ manifold; one with A' symmetry and two with A'' symmetry. A treatment identical to that of $B–H_2$ may be implemented.[37] It is useful to point out that in this case, the electron configuration of p^4 implies that in the ^3P term states the doubly occupied orbital is the unique one, accordingly, the subscript in the $p_{x,y,z}$ designation indicates the orientation of this orbital. The three adiabatic potential energy surfaces are designated $V_{1A'''}$, $V_{2A''}$, and $V_{A'}$. The diabatic basis (p_x, p_y, p_z) are used, with p_x and p_z lying in the $O–H_2$ plane. The functional forms for fitting the potential energy surface are

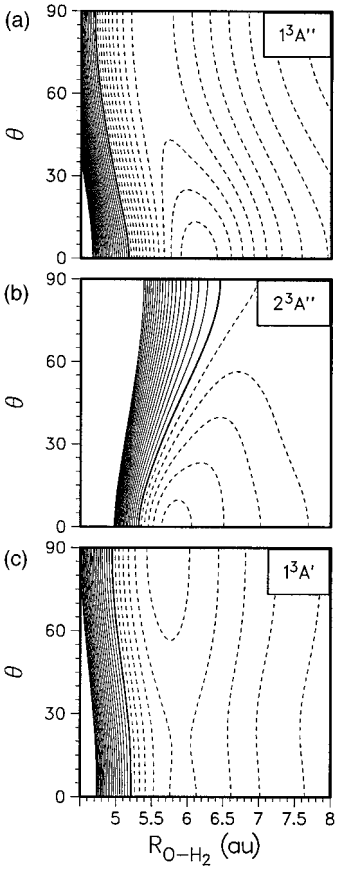

FIG. 2. Contour plots of the $O(^3P)$–H_2 adiabatic potential surfaces; (a) $1A''$; (b) $2A''$; (c) A'.

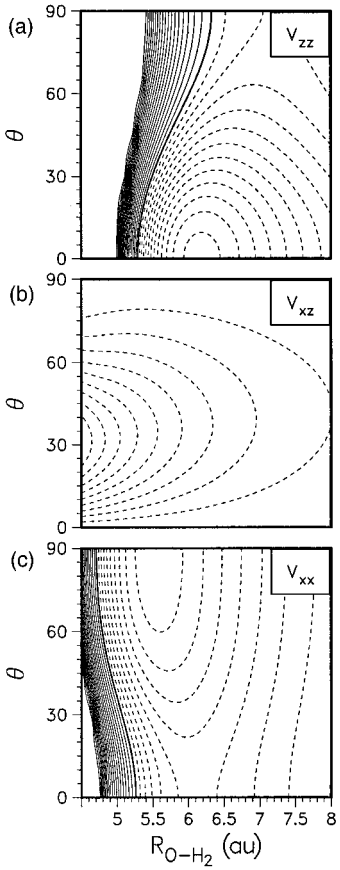

FIG. 3. Contour plots of the $O(^3P)$–H_2 diabatic potential surfaces; (a) V_{zz}; (b) V_{xz}; (c) V_{xx} (the V_{yy} surface is the same as A' in Fig. 2).

$$V^{zz}(R,\theta)=\sum_{L=0,2,4} V_L^{zz}(R)D_{0,0}^L(0,\theta,0),$$

$$V^{xx}(R,\theta)=\sum_{L=0,2,4} V_{L0}^{xx}(R)D_{00}^L(0,\theta,0) - V_{L2}^{xx}(R)D_{20}^L(0,\theta,0),$$

$$V^{yy}(R,\theta)=\sum_{L=0,2,4} V_{L0}^{xx}(R)D_{00}^L(0,\theta,0) + V_{L2}^{xx}(R)D_{20}^L(0,\theta,0), \quad (4)$$

and the nonadiabatic coupling term V^{xz} is

$$V^{xz}(R,\theta)=\sum_{L=0,2,4} V_L^{xz}(R)D_{10}^L(0,\theta,0). \quad (5)$$

The surfaces are therefore fitted with 60 parameters with an rms deviation of 5 cm^{-1}. The adiabatic potential energy surfaces and their fits in the diabatic representation are shown in Figs. 2(a), 2(b), and 2(c) and Figs. 3(a), 3(b), and 3(c), respectively. Note that V^{yy} corresponds to the A' adiabatic surface of Fig. 2, since the P_y orbital is perpendicular to the O–H_2 plane and does not mix with P_x and P_z.

3. ^1D state

For $O(^1D)$ atoms interacting with H_2 there are five sublevels; three with A' symmetry and two with A'' symmetry. The five diabatic basis functions can also be divided into two such groups, since $(d_{z^2}, d_{xz}, d_{x^2-y^2})$ belong to A' and (d_{xy}, d_{yz}) belong to A'' symmetry. 3×3 and 2×2 matrices are generated for the two groups. There are a total of nine independent matrix elements (six independent elements for the A' matrix and three for the A'' matrix). The diagonal terms can be expanded as

$$V(R,\theta)=\sum_{L=0,2,4,6} V_{L0}(R)D_{0,0}^L(0,\theta,0), \quad (6)$$

and the off-diagonal terms as

$$V(R,\theta)=\sum_{L=0,2,4,6} V_{L1}(R)D_{10}^L(0,\theta,0). \quad (7)$$

There are a total of 96 parameters in the global fit to the potential energy data, fitted with an RMS deviation of 6.1 cm^{-1}. The contour plots of the diabatic potential functions are not presented in the paper. In Appendix B, the pair potential curves of $O(^1D)$ interacting with a spherical D_2 are shown. These are obtained by averaging over the orientation of D_2.

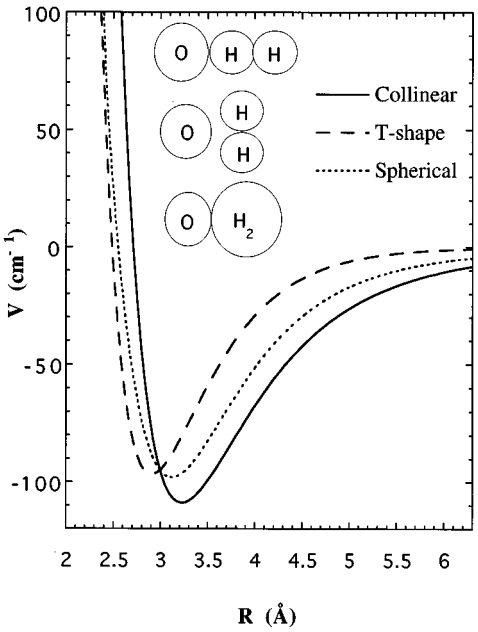

FIG. 4. The lowest adiabatic potential curves of $O(^3P)$–H_2 for linear, T-shaped, and spherically averaged geometries (see the text for details).

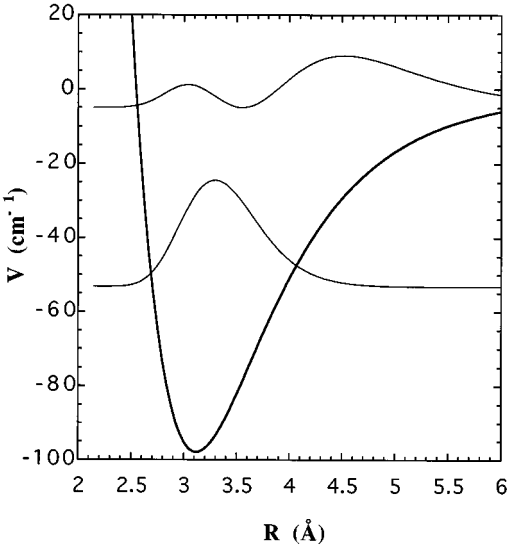

FIG. 5. Potential energy curve for $O(^3P)$–para-H_2 stretching coordinate and the probability density $|\Psi(R)|^2$ of the two bound eigenstates.

III. ROTATIONALLY ADIABATIC POTENTIAL ENERGY SURFACES FOR $O(^3P)$–H_2

In the ground electronic state of the system, magnetic dipole coupling between $O(^3P)$ and H_2, will lead to spin relaxation of the nearest-neighbor molecules within ~0.1 s.[40,41] All subsequent studies of the doped solid will therefore be limited to O atoms isolated in a cage of para-H_2 (ortho-D_2), i.e., to molecules with only even rotational states.[40] The anisotropy of the $O(^3P)$–H_2 interaction with respect to the H_2 orientation will determine whether the nearest-neighbor H_2 molecules can be regarded as free rotors, or strongly hindered rotors. In the former case, in the $J=0$ ground state, only the spherically averaged potentials have any meaning, while in the case of strong hindering, the angle dependence should be explicitly taken into account.

The anisotropy of the $O(^3P)$–H_2 interaction can be gauged from Fig. 4, where the adiabatic potential energy curves are shown, for collinear, $V_\Sigma(R)$, and T-shape, $V_\Pi(R)$, approaches. The spherically averaged potential $V_{j=0}(R)$ is also shown in the same figure. This potential supports two stretching states of the $O(^3P)$–H_2 complex, as shown in Fig. 5. The dissociation energy is approximately 50 cm^{-1}, and the equilibrium distance is 3.2 Å. Note, that the $v=0$ wave function spans the minima in both ''T'' and linear geometries. Fixing the distance of the O–H_2 complex at the minimum of the orientationally averaged potential, we solve the one-dimensional rotational Hamiltonian

$$H=-\frac{\hbar^2}{2I}\frac{\partial^2}{\partial\theta^2}+V(R_0,\theta), \tag{8}$$

in which I is the moment of inertia of H_2 and $V(R_0,\theta)$ is the rotational potential at $R_0=3.2$ Å, by expanding the wave function in the even plane harmonics

$$\psi(\theta)=\sum_m \frac{a_m}{\sqrt{2\pi}}e^{-im\theta};\quad m=0,\pm2,\pm4,\ldots\ . \tag{9}$$

The angular potential $V(R_0,\theta)$ is shown in Fig. 6, along with the angular probability $|\psi(\theta)|^2$. The barrier to rotation of H_2 in the complex is approximately 25 cm^{-1}, significantly smaller than the vibrational zero-point energy of 45 cm^{-1}. While the preferred orientation is the linear geometry, $\theta=0°$, there is substantial probability at $\theta=90°$. The probability ratio between T-shaped vs linear geometries of the complex, $|\psi(90°)|^2/|\psi(0°)|^2$, are 70% for H_2 and 50% for D_2. More meaningful are the squared coefficients of the expansion in Eq. (9), which are a measure of the purity of the rotational states of the molecule. In the case of H_2, $a_0^2=0.935$ while $(a_2^2+a_{-2}^2)=0.0646$, i.e., the ground state has 93% free rotor

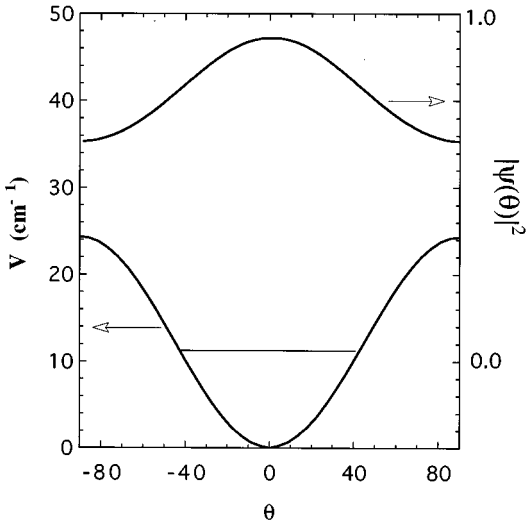

FIG. 6. Rotational barrier of H_2 in $O(^3P)$–H_2 complex and the probability density $|\Psi(\theta,R=R_0)|^2$ of the ground rotational state.

$J=0$ character, with only ~6% admixture from the first excited rotational level, $J=2$; and negligible contribution from higher states. In the case of deuterium, the excited state admixture is larger. Now, $J=0$ character is 83.8%, and the first excited state contribution is 17.1%. Two considerations further reduce this orientational localization, inclusion of the vibrational zero-point amplitude and the consideration that in the many-body system, due to the H_2–H_2 interactions, the orientational anisotropy will be further reduced. Thus, it is quite clear that even in the case of D_2, little error will be made by assuming the free rotor $J=0$ state to represent the ground state of the molecule. In short, in the ground state of the system, H_2 molecules can be regarded as spherical, and the use of orientationally averaged potentials are well justified. We adhere to this assumption in the rest of this paper.

IV. SIMULATION METHOD

We carry out semiclassical molecular dynamics simulations of $O(^3P, {}^1D)$ atoms in D_2 solid based on the parametrization of the global potentials, and after integrating out their θ dependence. The simulations do not assume additivity of potentials, but rather incorporate the anisotropic interactions of the open shell atom with the lattice by diagonalization of the potential matrix. The detailed description of the method has been given in Refs. 27 and 35, here we only present a brief outline.

The interaction Hamiltonian for an oxygen atom in the field of n close shell spherical D_2 molecules, in first order perturbation, can be expressed as[42]

$$H_{\rm int}=V_{\rm O-D_2}(r,R_1,R_2,\ldots,R_n)+V_{\rm D_2-D_2}(R_1,R_2,\ldots,R_n), \tag{10}$$

in which r and R represent, respectively, the electronic coordinate on the O atom and the coordinate of the spherical D_2 molecule as measured from the origin centered on the oxygen core. Note O has two valence holes which are treated as coupled in the atomic limit. The single variable r is used to represent the electronic degree of freedom as an effective charge distribution. Accordingly, we will denote its orbital angular momentum as $l\equiv L=l_1+l_2$, and $m\equiv M_L$. The angular dependence of $V_{\rm O-D_2}$ is then expanded in Legendre polynomials, $P_L(r\cdot R_k)$

$$V_{\rm O-D_2}(r,R_1,R_2,\ldots,R_n)=\sum_{k=1}^{n}\sum_{L=0}^{\infty}V_L(r,R_k)P_L(R_k\cdot r), \tag{11}$$

and the electronic eigenenergies are obtained by diagonalizing $V_{\rm O-D_2}$ in the uncoupled basis sets, $|lm>0\,|ns>_{\rm D_2}$; $l=1$ for $O(^3P)$; $l=2$ for $O(^1D)$. The closed shell ortho-D_2 molecular functions $|ns>_{\rm D_2}$, will be dropped from further explicit notation. Using the addition theorem for the expansion of the Legendre polynomial, $H_{\rm int}$ can be evaluated as the product of spherical harmonics

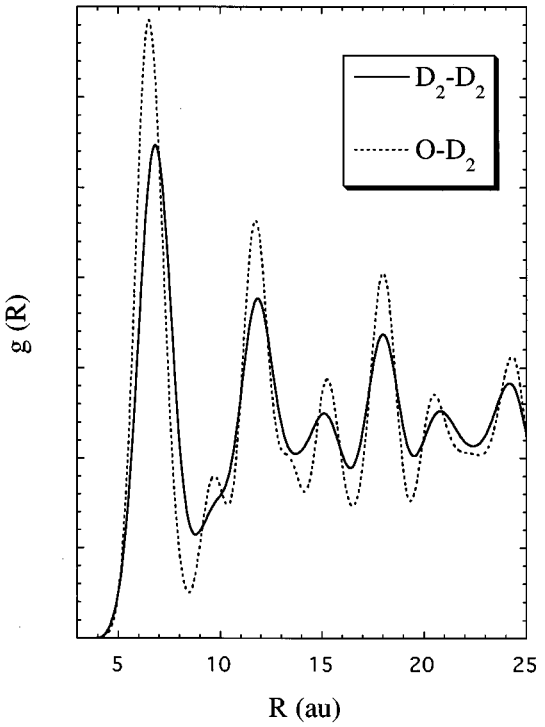

FIG. 7. Radial distribution functions of O–D_2 and D_2–D_2 for a system of $O(^3P)$ occupying a single substitutional site in an fcc D_2 solid at 4 K.

$$V_{mm}=\sum_{k=1}^{n}\sum_{L=0}^{\infty}\frac{4\pi}{2L+1}\left\langle Y_{lm}(\theta,\varphi)\right|\sum_{M=-L}^{L}Y_{LM}(\theta,\varphi)\times\left|Y_{lm}(\theta,\varphi)\right\rangle V_L(R_k)Y^*_{LM}(\theta_k,\varphi_k), \tag{12}$$

in which the subscript k refers to the D_2 molecules, of which there are n; the unsubscripted coordinates are for the O atom electron; and L is the order of the Legendre polynomial. The conditions $l+L+l=$even, and $l+L+l1\geqslant 0$, limit the summation over L. Only two terms, $L=0,2$, contributed in the case of $O(^3P)$, and only three terms, $L=0,2,4$, contribute in the case of (^1D). The individual matrix elements $V_{mm'}$, using the real ^1D basis set, are given explicitly in Appendix A.

Classical molecular dynamics simulations will be performed on the minimum energy surface of the diagonalized interaction Hamiltonian of the system. For the host, only ortho-$D_2(J=0)$ is considered. Pseudopotentials obtained by convolution of the zero-point wave function, as outlined in Ref. 22, are used to describe the D_2–D_2 interactions.

V. RESULTS AND DISCUSSIONS

A. Structure and stability of ground state $O(^3P)$ atom in solid D_2

First we carry out simulations of an fcc D_2 solid, with a single $O(^3P)$ atom as a substitutional impurity. Periodic boundary conditions are used and the system is equilibrated at 4 K for approximately 10 ps prior to sampling of the trajectories. Figure 7 shows the radial distribution function of D_2–D_2 and $O(^3P)$–D_2 in this system. The comparison makes

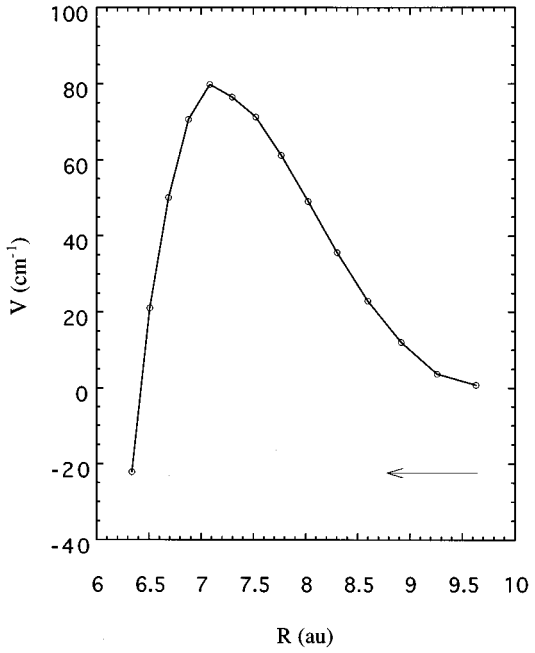

FIG. 8. Mean-field reaction barrier for next nearest-neighbor $O(^3P)+O(^3P)$ reaction in the fcc D_2 lattice.

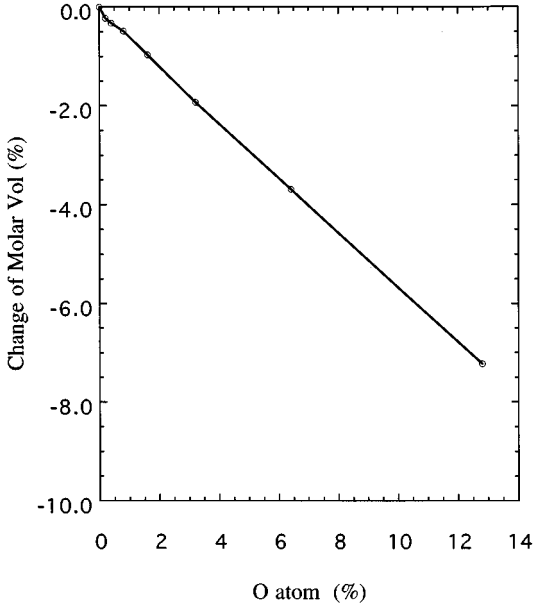

FIG. 9. Change of the molar volume as a function of O atom concentration in solid D_2.

it clear that the first shell of D_2 molecules are localized around $O(^3P)$ atoms, with ~10% increase in local density.

In considering solids with high concentration of dopants, it is crucial to establish the stability with respect to recombination of atoms. To this end, we consider the free energy barrier for recombination of a pair of O atoms initially placed in the lattice as second nearest neighbors. The total energy of the system as a function of separation between O atoms, and by allowing the lattice to fully relax at every step, is shown in Fig. 8. The mean-field reaction barrier is approximately 80 cm^{-1}. Two terms are expected to contribute to the barrier height, the reduced coordination number per oxygen atom and the work associated with the activation volume. These contributions are separated by a reference calculation, namely the mean potential for recombination of O atoms in a pair of $O(^3P)(D_2)_{12}$ clusters in the absence of the extended lattice. For this purpose, two icosahedral $O(^3P)(D_2)_{12}$ clusters were considered, with an initial O–O separation same as that of the second nearest neighbors in the host. The calculated mean-field barrier for recombination in the clusters is 40 cm^{-1}, nearly half that in the lattice. Quite clearly, the activation volume is positive, and the solid state recombination barrier can be expected to increase as a function of external pressure. Moreover, it is clear that at the relevant temperatures of 4 K, the solid can be doped at the few % level, without substantial recombination. We therefore calculate the molar volume of the solid as a function of $O(^3P)$ atom concentration. To ensure that the solid remains at zero external pressure, for each doping level, the volume of the cell is adjusted to minimize the total energy. The partial molar volume of the solid, $\delta V/\delta n$, is negative and linear. This is illustrated in Fig. 9, where it can be seen that the molar volume of a solid doped at the 4% level is ~2% less than that of the undoped solid. In effect the impurities stabilize the lattice.

B. Reactivity of excited state $O(^1D)$ atom in D_2 solid

Given the fact that the present potentials show that in the T approach the $O(^1D)$–H_2 potential is strictly reactive, the experimental observation of nonreaction on this surface in the solid state is rather intriguing. We examine whether this is a many-body effect, or whether the reaction barrier is eliminated in the $J=0$ state through rotational averaging. The rotationally averaged radial functions $V_L(R)$ are extracted from the rotationally averaged *ab initio* pair potentials using the following well-known relations[28]

$$\begin{aligned} V_0 &= \tfrac{1}{5}(V_\Sigma + 2V_\Pi + 2V_\Delta), \\ V_2 &= (V_\Sigma - V_\Pi) + (V_\Pi - V_\Delta), \\ V_4 &= \tfrac{9}{5}(V_\Sigma - V_\Pi) + \tfrac{3}{5}(V_\Delta - V_\Pi). \end{aligned} \tag{13}$$

The required pair potentials $V_\Sigma, V_\Pi, V_\Delta$ and their parametrization are given in Appendix B. (Note there are some typographical errors in Ref. 27).

Figure 10 shows the *ab initio* excited state potentials of $O(^1D)$ interacting with a spherical D_2 molecule. The three Legendre components, V_0, V_2, and V_4, are plotted as a function of distance between the O atom and the center of mass of D_2. Note, only V_0 is nonreactive, and therefore, only in spherically symmetric sites is the atom rigorously unreactive with its host. In O_h sites, V_2 may be ignored since its decomposition under the crystal field does not contain the totally symmetric representation. However, V_4 does, and contributions from V_0 and V_4 lead to the T_{2g} and E_g splitting of the ^1D surface. These surfaces are bound for an octahedral cluster, as shown in Fig. 11 for the breathing sphere coordi-

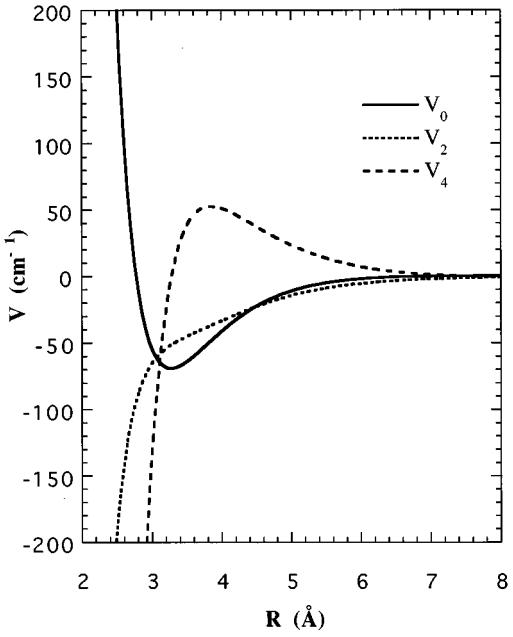

FIG. 10. Spherical components of potential energy functions for an $O(^1D)$ interacting with ortho-D_2 as a function of distance.

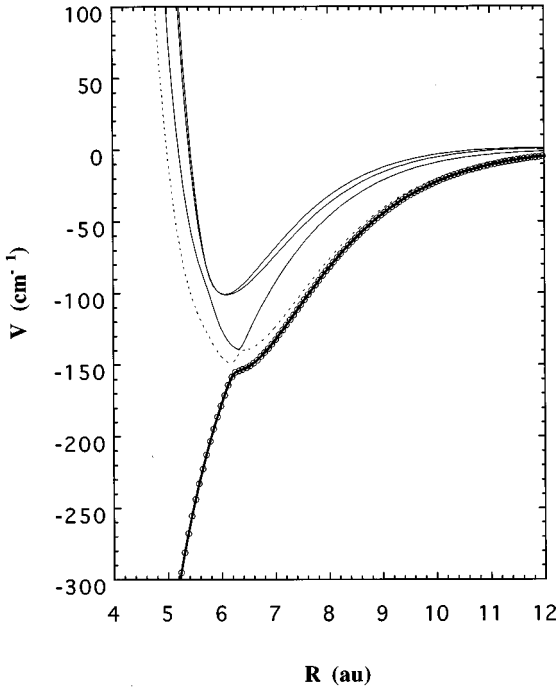

FIG. 12. Same as Fig. 11, except for $O(^1D)(D_2)_3$ cluster in D_{3h} symmetry.

nate. However, the bound character is accidental. In this case, at short distance, V_0 dominates over V_4. If the local site symmetry is further reduced, V_2 will also contribute. For instance, if we symmetrically arrange three D_2 molecules around $O(^1D)$ in a plane, i.e., in D_{3h} symmetry, then all three components contribute, and the resulting surface is reactive as shown in Fig. 12. The surfaces in Fig. 11 are deceptive, while in the symmetric breathing coordinate they are bound,

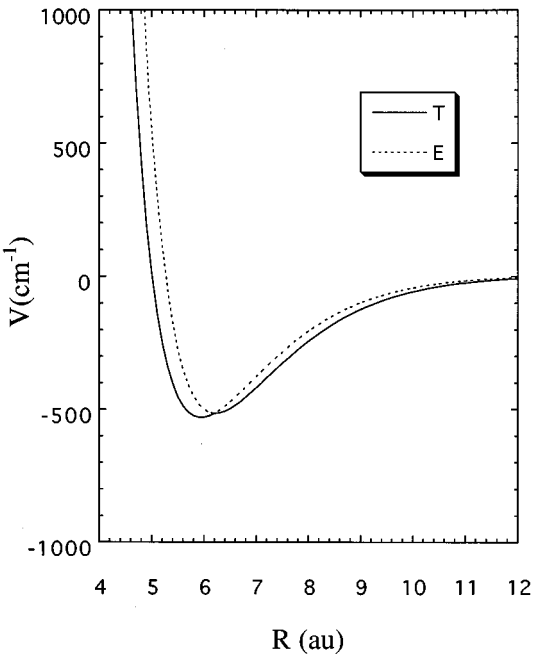

FIG. 11. Potential energy profile of the $O(^1D)$ manifold as a function of breathing sphere coordinate for the icosahedral $O(^1D)(D_2)_{12}$ cluster.

asymmetric vibrational modes do lead to reaction. The fragility of the binding character can be discerned from Fig. 10, where it can be seen that the V_4 and V_0 curves intersect very near the V_0 minimum. If this intersection were to occur on the right turning point, then even in spherical sites the overall potential would have been reactive. With the same token, if the intersection were to occur at a slightly shorter distance on the inner turning points, then at 4 K the system could be perfectly stable with respect to reaction. We amplify this point by carrying out a normal mode analysis of clusters, to elucidate the coordinates responsible for reaction.

C. Normal mode analysis

To carry out a normal mode analysis of an $O(D_2)_{12}$ cluster, we first search for the minimum energy configuration by simulated annealing, and then diagonalize the force matrix. The annealing procedure fails on the ^1D surface. Reaction occurs prior to lowering the temperature of the cluster. In an attempt to identify the reaction coordinates, we resorted to

TABLE I. Normal mode frequencies of $O(^3P)(D_2)_{12}$ cluster.

Frequency (cm^{-1})	Symmetry	Degeneracy
27.63	*H*	5
34.31	*F*	3
37.54	*G*	4
39.06	*H*	5
47.39	*F*	3
52.36	*G*	4
57.77	*H*	5
61.78	*A*	1
69.03	*F*	3

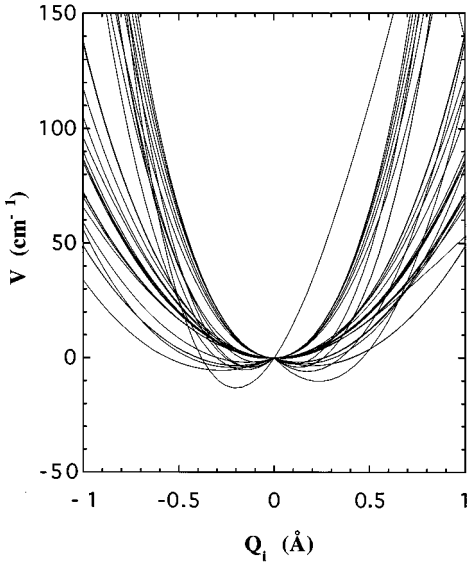

FIG. 13. Potential energies along the normal displacements of the $O(^1D)(D_2)_{12}$ cluster.

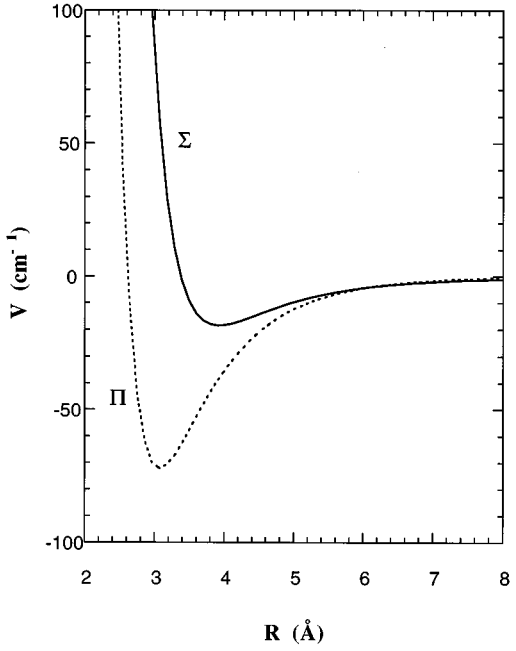

FIG. 15. Potential energy curves for $O(^3P)$ and spherical H_2.

first calculating the normal modes on the nonreactive ^3P surface, and then used the same coordinates to evaluate the potential energy curves on the ^1D surface. There are 33 normal modes for $O(^3P)(D_2)_{12}$, which can be classified according to the irreducible representations of I_h (icosahedral) symmetry. The frequencies of these modes and their degeneracy are listed in Table I. Using the same modes, the potential energy curves on the ^1D surface were evaluated as a function of normal displacement. These are shown in Fig. 13 to be entirely bound. Despite this seeming stability, finite temperature molecular dynamics simulations of the complex always lead to dissociation. This seeming contradiction is rationalized by noting that all of the modes are highly anharmonic and strongly coupled; moreover, it is clear that the reaction does not occur along a pure single normal coordinate but rather along combinations.

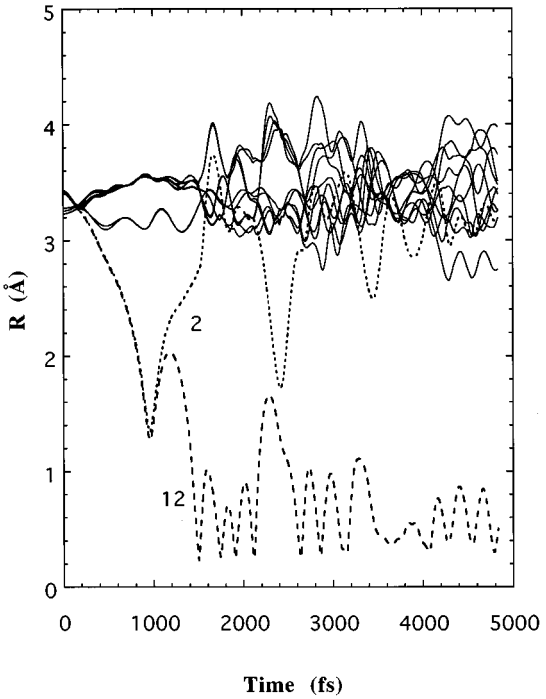

FIG. 14. MD simulation result which shows the distances between the $O(^1D)$ atom and 12 D_2 nearest neighbors in the $O(^1D)$ doped D_2 solid, see the text for details.

The reactivity of the cluster does not necessarily preclude the possibility that at low temperatures the system may be stable in the extended solid. To test this possibility, we carry out MD simulations that closely correspond to the experimental conditions. The solid is represented with a cell of 499 spherical D_2 molecules (atoms), with an O atom at a substitutional site. Periodic boundary conditions are used. The system is initially equilibrated on the ^1S state at an artificially low temperature (<0.01 K). The potential energy surface is then suddenly switched from ^1S to ^1D, and the dynamics is followed on the ^1D surface. A typical run is illustrated in Fig. 14, in which the time dependence of all twelve O–D_2 nearest-neighbor separations are shown. Trajectories 2 and 12 represent two D_2 molecules at opposite ends from each other. The attraction of these two atoms to the $O(^1D)$ atom is due to the locking of d_{z^2} orbital on $O(^1D)$ along this axis. This geometrical arrangement will result in two Σ-type interactions between $O(^1D)$ and D_2 which will lead to reaction (see Fig. 15). Note that in the first attempt along this coordinate, reaction failed. The reaction is blocked by crowding, the repulsive interactions among the D_2 molecules prevent the closer approach required for insertion. The reaction candidates are bounced back around 1.0 ps. Reaction occurs on the second attempt when one of the axial D_2 molecules, trajectory 12, undergoes insertion. Quite clearly,

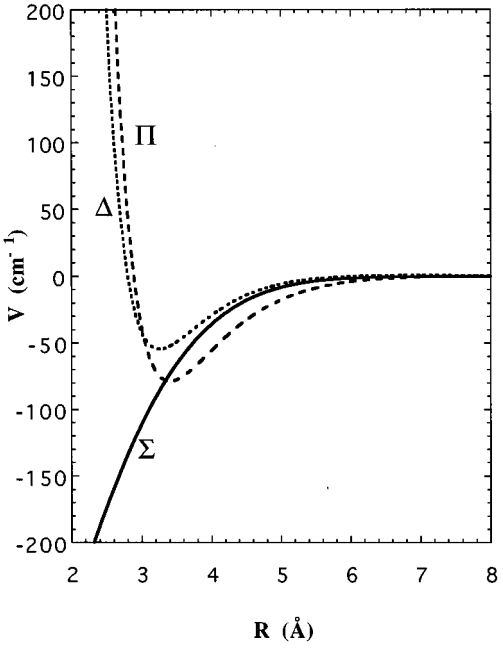

FIG. 16. Potential energy curves for $O(^1D)$ and spherical H_2.

from the stable initial configuration to the entrance channel for reaction a free energy barrier, that can be surmounted at 4 K, exists.

VI. CONCLUSION

We have carried out *ab initio* electronic structure calculations of the adiabatic potential energy surfaces of $O(^1S,^1D,^3P)+H_2$ and produced global fits to the surfaces using a limited basis diabatic representation. The formalism allows the calculation of energetics and dynamics on the minimum energy surfaces arising from each electronic term. It was established that description of the lattice as composed of spherical H_2 molecules is well justified for the ground state of the system. All calculations were therefore limited to solids of spherical ortho-D_2 or para-H_2 in $J=0$.

In the $O(^3P)$ ground state, at the relevant cryogenic temperatures, the doped solid is stable with respect to recombination of atoms. The activation energy for recombination is 120 K, and the activation volume is positive. The latter implies that the lattice can be further stabilized by the application of pressure. Moreover, it was shown that doping stabilizes the lattice by increasing its local density around the impurity. These conclusions are in qualitative agreement with recent experiments, where O atoms were photolytically generated in solid D_2, and it was observed that recombination only occurs under conditions where the entire solid starts to melt.[9]

Although somewhat stabilized in highly symmetric environments, $O(^1D)$ is found to be reactive in the solid even at 4 K. This result remains in contradiction with the experimental suggestion that the $O(^1D)+D_2$ reaction does not occur in the solid state.[9] The origin of this disagreement is not clear at present. The possibility that the observed $O(^1S\rightarrow{}^1D)$ emission in the experiment is due to O atoms complexed with O_2 has been suggested. However, even in that case it is not clear why $O(^1D)$ atoms do not disappear by reaction either with O_2 or H_2. Alternatively, it may be argued that the present treatment is not adequate for the analysis of chemistry under the experimental conditions. Indeed the spin–orbit Hamiltonian was left out of the *ab initio* calculations, and this may have a profound effect on chemistry at 4 K. The calculations were also limited to the minimum energy surfaces of each term state, and therefore, did no include intersystem crossing possibilities. However, it is highly doubtful that such a process could compete with the observed ps reaction time scale. In short, the issue of reactivity of $O(^1D)$ in solid H_2 remains unresolved in our minds.

ACKNOWLEDGMENTS

This research was made possible through an AFOSR grant, F49620-1-0251, under the University Research Initiative (Z.L. and V.A.A.) and the U.S. Department of Energy, Division of Chemical Sciences under Contract No. W-31-1109-Eng-38 (L.B.H.).

APPENDIX A: MATRIX ELEMENTS FOR THE INTERACTION HAMILTONIAN IN THE *D* BASIS SET

The explicit expression of matrix element $V_{mm'}$ for d basis set ($l=2$) have been given in a previous paper,[27] because there are some typographical errors there, we present the correct ones here. For computational purposes, we find it most convenient to use Cartesian coordinates, in a real basis set. For the d basis set

$$\begin{aligned}
&d_{z^2} \quad |1\rangle = Y_{2,0},\\
&d_{xy} \quad |2\rangle = (1/\sqrt{2})(Y_{2,2}+Y_{2,-2}),\\
&d_{x^2-y^2} \quad |3\rangle = (i/\sqrt{2})(-Y_{2,2}+Y_{2,-2}),\\
&d_{xz} \quad |4\rangle = (i/\sqrt{2})(Y_{2,1}+Y_{2,-1}),\\
&d_{yz} \quad |5\rangle = (1/\sqrt{2})(-Y_{2,1}+Y_{2,-1}),
\end{aligned} \tag{A1}$$

the interaction matrix V is real and symmetric ($V_{ij}=V_{ji}$) with elements

$$V_{11}=V_0-\frac{1}{7}\left[1-3\frac{z^2}{r^2}\right]V_2+\left[\frac{3}{28}-\frac{15}{14}\frac{z^2}{r^2}+\frac{5}{4}\frac{z^4}{r^4}\right]V_4,$$

$$V_{22}=V_0+\frac{1}{7}\left[1-3\frac{z^2}{r^2}\right]V_2+\left[\frac{1}{56}-\frac{5}{28}\frac{z^2}{r^2}-\frac{5}{24}\frac{(x^4+6x^2y^2-y^4-z^4)}{r^4}\right]V_4,$$

$$V_{33}=V_0+\frac{1}{7}\left[1-3\frac{z^2}{r^2}\right]V_2+\left[\frac{1}{56}-\frac{5}{28}\frac{z^2}{r^2}+\frac{5}{24}\frac{(-x^4+6x^2y^2-y^4+z^4)}{r^4}\right]V_4,$$

$$V_{44}=V_0-\frac{1}{14}\left[1+3\frac{(x^2-y^2-z^2}{r^2}\right]V_2+\left[\frac{1}{14}-\frac{5}{42}\frac{(x^2-y^2+6z^2)}{r^2}+\frac{5}{6}\frac{z^2(x^2-y^2+z^4)}{r^4}\right]V_4,$$

$$V_{55}=V_0-\frac{1}{14}\left[1-3\frac{(x^2-y^2+z^2]}{r^2}\right]V_2+\left[\frac{1}{14}+\frac{5}{42}\frac{(x^2-y^2-6z^2)}{r^2}-\frac{5}{6}\frac{z^2(x^2-y^2-z^4)}{r^4}\right]V_4,$$

$$V_{12}=[(-x^2+y^2)/\sqrt{3}r^2]\left[\frac{3}{7}V_2+\left(\frac{5}{28}-\frac{5}{4}\frac{z^2}{r^2}\right)V_4\right],$$

$$V_{13}=[xy/\sqrt{3}r^2]\left[-\frac{6}{7}V_2-\left(\frac{5}{14}-\frac{5}{2}\frac{z^2}{r^2}\right)V_4\right],$$

$$V_{14}=[yz/\sqrt{3}r^2]\left[\frac{3}{7}V_2-\left(\frac{15}{14}-\frac{5}{2}\frac{z^2}{r^2}\right)V_4\right],$$

$$V_{15}=[xz/\sqrt{3}r^2]\left[\frac{3}{7}V_2-\left(\frac{15}{14}-\frac{5}{2}\frac{z^2}{r^2}\right)V_4\right],$$

$$V_{23}=\frac{5}{6}\frac{xy(x^2-y^2)}{r^4}V_4,$$

$$V_{24}=\left[\frac{yz}{r^2}\right]\left[-\frac{3}{7}V_2-\left(\frac{5}{28}-\frac{15x^2-5y^2+5z^2}{12r^2}\right)V_4\right],$$

$$V_{25}=\left[\frac{xz}{r^2}\right]\left[\frac{3}{7}V_2+\left(\frac{5}{28}+\frac{5x^2-15y^2-5z^2}{12r^2}\right)V_4\right],$$

$$V_{34}=\left[\frac{xz}{r^2}\right]\left[\frac{3}{7}V_2+\left(\frac{5}{28}+\frac{-5x^2+15y^2-5z^2}{12r^2}\right)V_4\right],$$

$$V_{35}=\left[\frac{yz}{r^2}\right]\left[\frac{3}{7}V_2+\left(\frac{5}{28}+\frac{15x^2-5y^2-5z^2}{12r^2}\right)V_4\right],$$

$$V_{45}=\left[\frac{xy}{r^2}\right]\left[\frac{3}{7}V_2-\left(\frac{5}{21}-\frac{5z^2}{3r^2}\right)V_4\right],$$

where $r^2=x^2+y^2+z^2$ and V_0, V_2, and V_4 are the radial potential energy functions associated with the Legendre expansion in Eq. (10) of the text.

APPENDIX B: POTENTIAL ENERGY FUNCTIONS FOR O(^3P, ^1D) INTERACTING WITH A SPHERICAL D_2

The pair interaction potential energy functions between O(^3P, ^1D) and a spherical H_2 or D_2 are obtained by averaging the interaction potential functions over the orientation of the H_2 molecule. There are two potential energy curves for O(^3P)–D_2 shown in Fig. 15, and three for O(^1D)–D_2 as shown in Fig. 16. In the first case, V_Σ is for p_z and V_Π for p_x, p_y where the subscripts identify the orientation of the doubly occupied orbital. This explains the characters of these two curves, V_Σ is shallower, because of the earlier onset of repulsion between the filled atomic orbital and the closed molecular shell. In the case of O(^1D), V_Σ is for d_{z^2}, V_Π for d_{xy}, d_{vz}, and V_Λ for $d_{xy}, d_{x^2-y^2}$ (V_Π and V_Δ are doubly degenerate).

[1] A. M. Bass and H. P. Broida, *Formation and Trapping of Free Radicals* (Academic, New York, 1960).
[2] G. J. Minkoff, *Frozen Free Radicals* (Interscience, New York, 1960).
[3] M. E. Fajardo, S. Tam, T. L. Thompson, and M. E. Cordonnier, Chem. Phys. **189**, 351 (1994).
[4] Proceedings of the High Energy Density Matter (HEDM) Contractors' Conference, edited by T. L. Thompson (Woods Hole, MA 1993).
[5] D. C. Chatfield, R. S. Friedmen, G. C. Lynch, D. G. Truhlar, and D. W. Schwenke, J. Chem. Phys. **98**, 342, (1993), and references therein.
[6] K. Mikulecky and K. H. Gericke, J. Chem. Phys. **96**, 7490 (1992), and references therein.
[7] (a) G. H. Dieke and H. M. Crosswhite, J. Quant. Spectrosc. Radiat. Transfer **2**, 97 (1962); (b) J. A. Davidson, C. M. Sadowski, H. I. Schiff, G. E. Streit, C. J. Howard, D. A. Jennings, and A. L. Schmeltekopf, J. Chem. Phys. **64**, 57 (1976); (c) R. F. Heidner and D. Husain, Int. J. Chem. Kinet. **5**, 819 (1973); L. J. Steif, W. A. Payne, and R. B. Klemm, J. Chem. Phys. **62**, 4000 (1975); (d) R. A. Young, G. Black, and T. G. Slanger, *ibid*. **49**, 475 (1986).
[8] (a) P. A. Whitlock, J. T. Muckerman, and E. R. Fisher, J. Chem. Phys. **76**, 4468 (1982); (b) G. Durand and X. Chapuisat, Chem. Phys. **96**, 381 (1985); (c) M. S. Fitzcharles and G. C. Schatz, J. Phys. Chem. **90**, 3734 (1986); J. K. Badenhoop, H. Koizumi, and G. C. Scahtz, J. Chem. Phys. **91**, 142, (1989); (d) E. M. Goldfield and J. R. Wiesenfeld, *ibid*. **93**, 1030 (1990); (e) P. J. Kuntz, B. I. Niefer, and J. J. Sloan, *ibid*. **88**, 3629 (1988); Chem. Phys. **151**, 77 (1991).
[9] A. Danilychev, S. Tanaka, H. Kajihara, S. Koda, and V. A. Apkarian (in preparation).
[10] The quantum nature of a host is characterized by the de Boer parameter, J. de Boer, Physica **14**, 139 (1948).
[11] (a) M. E. Fajardo, S. Tam, T. L. Thompson, and M. E. Cordonnier, Chem. Phys. **189**, 351 (1994); (b) T. Momose, M. Uchida, N. Sogoshi, M. Miki, S. Masuda, and T. Shida, Chem. Phys. Lett. **246**, 583 (1995); T. Momose, M. Miki, M. Uchida, T. Shimizu, I. Yoshizawa, and T. Shida, J. Chem. Phys. **103**, 1400 (1995).
[12] (a) Q. Hui, J. L. Persson, J. H. M. Beijersbergen, and M. Takami, Laser Chemistry, **15**, 221 (1995); (b) S. I. Kanorsky, M. Arndt, R. Dziewior, and A. Weis, Phys. Rev. B **49**, 3645 (1994); (c) B. Tabbert, M. Beau, H. Gunther, W. Haubler, C. Honninger, K. Meyer, B. Plagemann, and G. zu Putlitz, Z. Phys. B **97**, 425 (1995).
[13] (a) R. Frochtenicht, J. P. Toennies, and A. Vilesov, Chem. Phys. Lett. **229**, 1 (1994); A. Scheidemann, B. Schilling, J. P. Toennies, and J. A. Northby, Physica B **165**, 135 (1990); (b) F. Stienkemeier, J. Higgins, W. E. Ernst, and G. Scoles, Z. Phys. B-Condensed Matter, **98**, 413 (1995); Phys. Rev. Lett. **74**, 3592 (1995); J. Chem. Phys. **102**, 615 (1995); S. Goyal, D. L. Schutt, and G. Scoles, J. Phys. Chem. **97**, 2236 (1993); S. Goyal, D. L. Schutt, G. Scoles, and G. N. Robinson, Chem. Phys. Lett. **196**, 123 (1992).
[14] M. E. Fajardo, J. Chem. Phys. **98**, 110 (1993).
[15] D. Scharf, G. J. Martyna, and M. L. Klein, J. Chem. Phys. **99**, 8997 (1993).
[16] D. Scharf, G. J. Martyna, D. Li, G. A. Voth, and M. L. Klein, J. Chem. Phys. **99**, 9013 (1993).
[17] K. B. Whaley, Inter. Rev. Phys. Chem. **13**, 41 (1994); R. N. Barnett and K. B. Whaley, J. Chem. Phys. **94**, 2953 (1992); **99**, 9730 (1993).
[18] J. B. Anderson, J. Chem. Phys. **63**, 1499 (1975).
[19] D. Blume, M. Lewrenz, F. Huisken, and M. Kaloudis, J. Chem. Phys. (submitted).
[20] V. Buch, J. Chem. Phys. **100**, 7610 (1994).
[21] *Monte Carlo Methods in Statistical Physics, Topics in Applied Physics 71*, edited by K. Binder (Springer, New York, 1992).
[22] (a) M. Sterling, Z. Li, and V. A. Apkarian, J. Chem. Phys. **103**, 5679 (1995); (b) Z. Li and V. A. Apkarian, J. Chem. Phys. (submitted).
[23] J. Cao and G. A. Voth, J. Chem. Phys. **99**, 10070 (1993); **100**, 5106 (1994); **101**, 6157 (1994).
[24] J. A. Cao and G. A. Voth, J. Chem. Phys. **101**, 6168 (1994).
[25] M. Pavese and G. A. Voth, Chem. Phys. Lett. **249**, 231 (1996).
[26] A. V. Danilychev, V. E. Bondybey, V. A. Apkarian, S. Tanaka, H. Kajihara, and S. Koda, J. Chem. Phys. **103**, 4292 (1995).

[27] A. V. Danilychev and V. A. Apkarian, J. Chem. Phys. **100**, 5556 (1994).
[28] V. Aquilanti, R. Candori, and F. Pirani, J. Chem. Phys. **89**, 6157 (1988).
[29] MOLPRO is a package of *ab initio* programs written by H.-J. Werner and P. J. Knowles, with contributions from J. Almlof, R. D. Amos, M. J. O. Deegan, S. T. Elbert, C. Hampel, W. Meyer, K. Peterson, R. Pitzer, A. J. Stone, and P. R. Taylor.
[30] H.-J. Werner and P. J. Knowles, J. Chem. Phys. **82**, 5053 (1985); P. J. Knowles and H.-J. Werner, Chem. Phys. Lett. **115**, 259 (1985).
[31] H.-J. Werner and P. J. Knowles, J. Chem. Phys. **89**, 5803 (1988); P. J. Knowles and H.-J. Werner, Chem. Phys. Lett. **145**, 514 (1988).
[32] R. Shepard, I. Shavitt, R. M. Pitzer, D. C. Comeau, M. Pepper, H. Lischka, P. G. Szalay, R. Ahlrichs, F. B. Brown, and J.-G. Zhao, Int. J. Quantum Chem. Symp. **22**, 149 (1988).
[33] S. R. Langhoff and E. R. Davidson, Int. J. Quantum Chem. **8**, 61 (1974); D. W. Silver and E. R. Davidson, Chem. Phys. Lett. **52**, 403 (1978).
[34] T. H. Dunning, Jr., J. Chem. Phys. **90**, 1007 (1989); R. A. Kendall, T. H. Dunning, Jr., and R. J. Harrison, *ibid.* **96**, 6796 (1992); D. E. Woon and T. H. Dunning, Jr., *ibid.* **98**, 1358 (1993).
[35] W. G. Lawrence and V. A. Apkarian, J. Chem. Phys. **101**, 1820 (1994).
[36] M. H. Alexander and M. Yang, J. Chem. Phys. **103**, 7956 (1995).
[37] M. H. Alexander, J. Chem. Phys. **99**, 6014 (1993).
[38] M. E. Rose, *Elementary Theory of Angular Momentum* (Wiley, New York, 1957).
[39] The potential parameters are available from the authors.
[40] I. F. Silvera, Rev. Mod. Phys. **52**, 393 (1980).
[41] The order of magnitude for the relaxation times is the same as for any paramagnetic center, of which T and H induced conversions are particularly well characterized, see for example: J. D. Sater, J. R. Gaines, E. M. Fearon, P. C. Souers, F. E. McMurphy, and E. R. Mapoles, Phys. Rev. B **37**, 1482 (1988); V. Shevtsov, A. Frolov, I. Lukashevich, E. Ylinen, P. Malmi, and M. Punkinnen, J. Low Temp. Phys. **95**, 815 (1994).
[42] See, for example, W. E. Baylis, J. Phys. B **10**, L477 (1977).